BRAINNORMALIZER: ANATOMY-INFORMED PSEUDO-HEALTHY BRAIN RECONSTRUCTION FROM TUMOR MRI VIA EDGE-GUIDED CONTROLNET

Min Gu Kwak

Department of Health and Rehabilitation Sciences
University of Pittsburgh
Pittsburgh, PA, USA

H. Milton Stewart School of Industrial and Systems Engineering Georgia Institute of Technology Atlanta, GA, USA

Yeonju Lee

H. Milton Stewart School of Industrial and Systems Engineering Georgia Institute of Technology Atlanta, GA, USA

Hairong Wang

Operations Research and Industrial Engineering, Cockrell School of Engineering
University of Texas at Austin
Austin, TX, USA

H. Milton Stewart School of Industrial and Systems Engineering Georgia Institute of Technology Atlanta, GA, USA

Jing Li

H. Milton Stewart School of Industrial and Systems Engineering Georgia Institute of Technology Atlanta, GA, USA

November 18, 2025

ABSTRACT

Brain tumors are among the most clinically significant neurological diseases and remain a major cause of morbidity and mortality due to their aggressive growth and structural heterogeneity. As tumors expand, they induce substantial anatomical deformation that disrupts both local tissue organization and global brain architecture, complicating diagnosis, treatment planning, and surgical navigation. Yet a subject-specific reference of how the brain would appear without tumor-induced changes is fundamentally unobtainable in clinical practice. We present BrainNormalizer, an anatomy-informed diffusion framework that reconstructs pseudo-healthy MRIs directly from tumorous scans by conditioning the generative process on boundary cues extracted from the subject's own anatomy. This boundary-guided conditioning enables anatomically plausible pseudo-healthy reconstruction without requiring paired non-tumorous and tumorous scans. BrainNormalizer employs a two-stage training strategy. The pretrained diffusion model is first adapted through inpainting-based fine-tuning on

tumorous and non-tumorous scans. Next, an edge-map-guided ControlNet branch is trained to inject fine-grained anatomical contours into the frozen decoder while preserving learned priors. During inference, a deliberate misalignment strategy pairs tumorous inputs with non-tumorous prompts and mirrored contralateral edge maps, leveraging hemispheric correspondence to guide reconstruction. On the BraTS2020 dataset, BrainNormalizer achieves strong quantitative performance (FID 27.1, SSIM 0.76, and a 7.1 percent false-positive detection rate) and qualitatively produces anatomically plausible reconstructions in tumor-affected regions while retaining overall structural coherence. BrainNormalizer provides clinically reliable anatomical references for treatment planning and supports new research directions in counterfactual modeling and tumor-induced deformation analysis.

Keywords Diffusion model; ControlNet; Pseudo-healthy brain MRI reconstruction; Edge-guided conditioning;

1 Introduction

Brain tumors are among the most life-threatening and clinically significant neurological diseases that affect individuals across all age groups worldwide [1, 2]. Their aggressive biological behavior and structural heterogeneity lead to severe neurological impairments and poor clinical outcomes, making them a major cause of morbidity and mortality [3]. This inherent complexity poses significant challenges for both clinical interpretation and computational analysis [4]. Furthermore, it leads to profound alterations in the structural and functional organization of the brain, thereby complicating accurate diagnosis and treatment planning [5, 6]. Magnetic Resonance Imaging (MRI) has become the primary modality for brain tumor assessment due to its superior soft-tissue contrast, high spatial resolution, and radiation-free imaging capability compared with Computed Tomography (CT) or other modalities [7, 8]. MRI enables detailed visualization of tumor-induced deformations and subtle structural variations in surrounding healthy tissues, which makes it indispensable for diagnosis, treatment planning, and surgical guidance [9].

Accurate interpretation of brain MRIs is essential for multiple aspects of clinical care, including tumor delineation, treatment planning, and surgical decision-making [10]. Clinicians use these images to plan resection strategies, determine radiation therapy targets, and predict potential risks to functional areas. However, because every brain exhibits unique structural variability, distinguishing tumor-induced changes from a patient's inherent neuroanatomy remains challenging [11]. Knowledge of the patient's pre-tumor brain would enhance these clinical tasks by providing a personalized reference for comparison [5]. Such a reference would enable more precise tumor delineation by clarifying which structures have been displaced or infiltrated, better assessment of how individual anatomical organization has been affected, and more confident identification of functional regions at risk [12].

Despite this need, obtaining healthy brain MRIs from patients is inherently challenging [13]. Patients rarely undergo MRI scans before symptom onset, as imaging is typically performed only after neurological symptoms appear. Moreover, the high cost of MRI examinations and the lack of insurance coverage for routine screening make it impractical to acquire longitudinal scans in healthy individuals [14]. Consequently, paired scans of the same patient in both pre-tumor and tumorous states are almost impossible. The absence of paired pre-tumor and tumorous scan datasets restricts the ability to quantify subject-specific structural deformations and conduct longitudinal studies [13]. This scarcity creates a strong motivation to computationally synthesize counterfactual reconstructions that capture not only the absence of the tumor but also a plausible restoration of surrounding anatomy. In other words, generating a pseudo-healthy MRI that reflects how the patient's brain would appear in the absence of tumor-induced alterations becomes necessary for enabling subject-specific analyses.

Generating high-quality images is inherently challenging because visual data contain complex contextual and structural relationships that must remain semantically and spatially consistent. Traditional generative models, such as Generative Adversarial Networks (GANs) [12, 15] and autoencoder-based frameworks [16, 17], have shown potential in image synthesis but often suffer from instability, mode collapse, and texture distortion, which reduce structural fidelity [18, 19]. In medical imaging, these challenges become even more pronounced because anatomical consistency and spatial precision are critical for clinical interpretation [20].

Recently, diffusion models have emerged as a transformative paradigm in image generation [21], demonstrating remarkable stability and realism across diverse domains. A diffusion model generates images by iteratively denoising random noise to reconstruct the underlying data distribution. This enables gradual refinement and robust learning even with limited data due to its stochastic and likelihood-based training nature. Since their introduction, diffusion models have evolved from denoising diffusion probabilistic models (DDPMs) [21] to more efficient variants such as denoising diffusion implicit models (DDIMs) [22] and latent diffusion models (LDMs) [23]. These advances have substantially improved generation quality and computational efficiency while maintaining semantic coherence. Stable Diffusion (SD), a LDM-based framework, has been widely used for image synthesis due to its ability to generate high-quality and semantically coherent images from text prompts through efficient latent-space denoising and text-guided conditioning

[23]. However, existing SD-based frameworks still lack mechanisms for fine-grained spatial control, which limits their ability to preserve detailed spatial correspondence and subject-specific structure. ControlNet addressed this limitation by incorporating auxiliary structural conditions such as edge, segmentation, or depth maps, which allow spatially precise and semantically guided image synthesis.

Owing to their strong generative capability and robustness to limited training data, diffusion models have rapidly gained attention in medical imaging research for their ability to produce realistic and anatomically consistent images [24]. They have been applied to a wide range of tasks, including image synthesis, translation, segmentation, and anomaly detection. For instance, Khader et al. applied Denoising Diffusion Probabilistic Models (DDPMs) for synthesizing MRI and CT images [25], while Ozbey et al. demonstrated cross-modality medical image translation. Diffusion models have also been utilized for segmentation tasks [26], and general medical image classification [27]. Moreover, Wolleb et al. employed a diffusion-based approach for anomaly detection [28]. Recent studies have also incorporated anatomical priors into diffusion-based medical image generation using structure-aware control frameworks such as ControlNet [29, 30, 31]. These approaches enhance anatomical fidelity through spatial conditioning with edge maps, segmentation priors, or shape constraints. However, research explicitly addressing pseudo-healthy MRI generation from tumorous scans remains limited, and patient-specific anatomically guided reconstruction has yet to be fully explored.

In this study, we present BrainNormalizer, a ControlNet-based diffusion framework designed to reconstruct subject-specific pseudo-healthy brain MRIs from tumorous scans while maintaining anatomical fidelity. Our model generates pseudo-healthy brain structures through a two-stage training scheme. In the first stage, an inpainting-based fine-tuning scheme adapts the pretrained diffusion model from natural images to the MRI domain, enabling anatomically coherent reconstruction of pseudo-healthy and tumorous tissues. In the second stage, the ControlNet branch is trained with structural cues extracted from edge maps, which highlight key anatomical boundaries such as cortical folds, ventricular contours, and major tissue interfaces. Conditioning the diffusion process on these boundary cues constrains generation to follow stable neuroanatomical geometry. This helps yield pseudo-healthy reconstructions that are more anatomically plausible and structurally consistent than those produced by unconstrained diffusion alone. During inference, counterfactual pseudo-healthy brain generation is achieved by deliberately misaligning tumorous MRIs with non-tumorous guidance through non-tumorous prompts and mirrored contralateral edge maps. This design leverages contralateral structural cues to generate anatomically consistent and clinically interpretable reconstructions without requiring paired scans from pre-tumor and tumorous states. The main contributions of this study are summarized as follows:

- Anatomy-informed diffusion framework for pseudo-healthy brain reconstruction. We propose BrainNormalizer, a diffusion-based framework that reconstructs pseudo-healthy brain MRIs by conditioning generation on anatomical boundary cues extracted from edge maps. These cues highlight stable structural patterns, which enables the diffusion process to adhere more closely to the subject's underlying neuroanatomy during pseudo-healthy reconstruction. Through progressive domain adaptation of pretrained diffusion models and edge-guided ControlNet training, the framework produces anatomically plausible pseudo-healthy images without requiring paired pre-tumor and tumorous scans.
- Counterfactual pseudo-healthy brain generation through deliberate misalignment. We generate counterfactual pseudo-healthy brains from tumorous MRIs by deliberately misaligning tumorous inputs with pseudo-healthy guidance signals. By providing non-tumorous prompts and mirrored contralateral edge maps, the model generates anatomically faithful reconstructions.
- Clinical and research implications for brain tumor assessment and treatment planning. From a clinical perspective, BrainNormalizer offers anatomically consistent reference images that approximate how the subject's brain might appear without tumor-induced changes, thereby serving as a pseudo-healthy structural baseline. This facilitates more accurate tumor delineation, supports preoperative planning that preserves critical regions, and enables postoperative and longitudinal evaluations. Furthermore, by generating anatomically reliable pairs of pseudo-healthy and tumorous MRI, BrainNormalizer provides valuable resources for downstream studies, including longitudinal analysis, counterfactual modeling, and quantitative assessment of tumor-induced deformation.

2 Related Works

2.1 Diffusion models for medical imaging tasks

Diffusion models have been applied for medical image analysis across diverse tasks and imaging modalities [32, 33, 34, 25, 35, 36, 28, 37, 38]. Hung et al. proposed Med-cDiff, a conditional diffusion probabilistic model for medical image super-resolution, denoising, and inpainting [32]. Zhang et al. proposed DiffuSeg, a conditional diffusion model

that synthesizes medical images from label maps and unlabeled target-domain data to mitigate annotation costs and improve segmentation performance across domains [34]. Khader et al. proposed a diffusion probabilistic framework for synthesizing realistic and anatomically consistent medical images from MRI and CT data [25]. Beyond image synthesis, diffusion-generated data have also been utilized to enhance segmentation, leveraging their probabilistic and generative nature to enable step-wise refinement and anatomically consistent predictions across modalities [36]. Furthermore, Wolleb et al. introduced a weakly supervised anomaly detection framework based on DDIM, using deterministic noising—denoising with classifier guidance to translate between tumorous and pseudo-healthy images and produce detailed anomaly maps without complex training [28]. Furthermore, with the advent of large language models (LLMs), text-to-image diffusion models have been introduced [37, 38], allowing intuitive and semantic control of generated images through text prompts.

Although diffusion models have achieved remarkable success in medical imaging tasks, their ability to preserve and control fine anatomical details remains still limited. In medical imaging, where subtle structural cues and precise tissue boundaries are crucial for clinical interpretation, such loss of detail can lead to anatomically implausible results. This limitation highlights the need for structure-guided diffusion frameworks capable of maintaining high-fidelity fine details during synthesis.

2.2 ControlNet

Researchers have investigated to control diffusion models on various forms of external information, such as class labels, textual prompts, or structural maps, to achieve controlled image generation. Such conditional diffusion frameworks enable both semantic and spatial guidance. Among these approaches, ControlNet has emerged as a powerful framework that injects structural conditions into large pretrained diffusion models while preserving their generative capabilities [35]. ControlNet is an end-to-end framework that conditions large pretrained text-to-image diffusion models on external structural signals such as edges, segmentation maps, or keypoints [35]. In this architecture, a trainable control branch is attached to a frozen diffusion backbone via zero-convolution layers, whose weights are initialized to zero to ensure that new control pathways gradually emerge during training without disrupting pretrained knowledge. The control branch processes these conditional inputs in parallel with the main diffusion stream and fuses them at multiple resolutions. This design allows spatially guided generation that preserves fine structural details while maintaining global semantic coherence.

ControlNet has inspired a number of extensions in medical imaging, where preserving anatomical consistency is essential. Konz et al. proposed a ControlNet-based diffusion model for breast MRI generation, where multi-class anatomical segmentation masks served as spatial guidance during sampling [29]. Wang et al. propose 3D MedDiffusion, demonstrating the strong potential of diffusion-based frameworks for CT and MRI tasks, where control is applied through depth and spatial structure conditions. Zhao et al. introduced a locally controllable diffusion framework for image generation that enables region-specific conditioning through regional discriminate loss and feature mask constraints with ControlNet [39]. Furthermore, Rue et al. applied a ControlNet framework for lung MRI-to-CT translation [40], using multi-channel conditioning that combined edge maps and intensity-normalized representations to improve alignment of structural boundaries. Qiu et al. incorporated ControlNet to improve medical image segmentation, enforcing image—mask consistency via a noise consistency loss [41].

While these approaches demonstrate ControlNet's potential for preserving fine structural information, their adaptation to medical imaging remains limited. Most existing works have focused on general image generation or domain translation rather than pathology-to-pseudo-healthy reconstruction. Extending structure-guided diffusion toward anatomically accurate and subject-specific restoration therefore remains an open research direction.

2.3 Medical image synthesis for pseudo-healthy MRI generation

Recent studies have explored transforming pathological medical images into their pseudo-healthy counterparts while preserving structural coherence. Liu et al. leveraged GANs to generate pseudo-healthy images, where lesion regions were inpainted to synthesize pseudo-healthy data [42]. Moving beyond GAN-based methods, diffusion frameworks have recently emerged as a more controllable and anatomically consistent alternative. Wolleb et al. introduced a weakly supervised anomaly detection framework based on DDIM that combines deterministic noising—denoising with classifier guidance to translate between tumorous and pseudo-healthy images and generate detailed anomaly maps without complex training [28]. However, since this method is not inpainting-based, it is less effective in reconstructing anatomically coherent pseudo-healthy tissue. Durrer et al. proposed a 2D diffusion-based pseudo-healthy reconstruction model [43]. Kwark et al. presented a hierarchical diffusion framework with perpendicular coarse-to-fine 2D stages to enhance inpainting consistency, yet both lacked explicit anatomical guidance [44]. Ferreira et al. introduced a wavelet diffusion approach to better preserve structural details, though it remained limited in anatomical awareness [45].

Despite these advances, existing pseudo-healthy MRI generation studies primarily focus on translating pathological regions into visually pseudo-healthy tissue without ensuring structural fidelity. Most diffusion-based methods perform inpainting or reconstruction without explicit anatomical guidance, often resulting in smooth but anatomically inconsistent reconstructions. Therefore, a diffusion framework that integrates structure-aware guidance for anatomically reliable pseudo-healthy generation remains lacking.

3 Materials and Methods

3.1 Overview

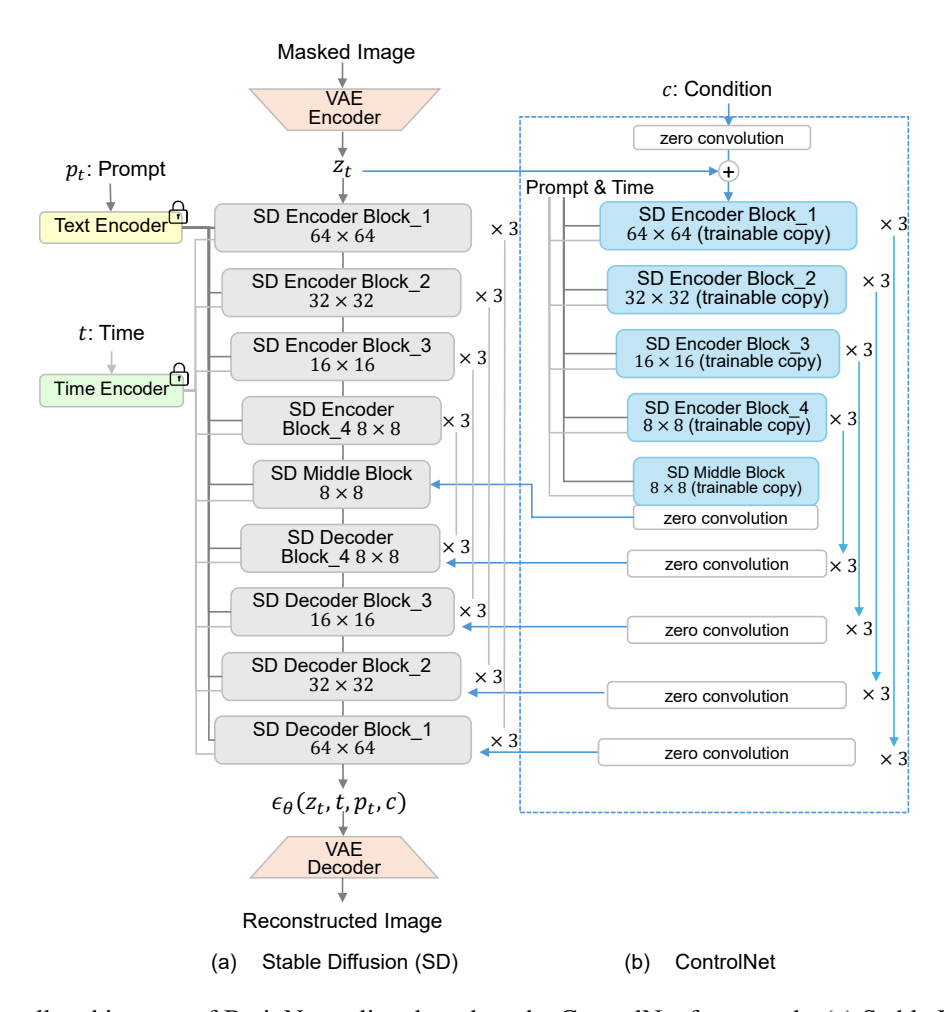


Figure 1: Overall architecture of BrainNormalizer based on the ControlNet framework. (a) Stable Diffusion (SD) backbone that performs latent-space denoising conditioned on text and time embeddings. (b) ControlNet branch that processes structural edge maps and injects boundary-aware features into the frozen SD decoder via zero-convolution layers. **Abbreviations:** VAE, Variational Autoencoder; SD, Stable Diffusion.

We propose BrainNormalizer, a ControlNet-based model that reconstructs subject-specific pseudo-healthy MRIs by restoring anatomy in tumor-affected regions while preserving the subject's own structural boundaries. The overall architecture of BrainNormalizer follows the ControlNet framework, which integrates a text-to-image SD backbone with a parallel control branch as illustrated in Figure 1. The SD component encodes a masked MRI image into a latent representation through a variational autoencoder (VAE) and progressively denoises it using a U-Net structure that incorporates both text embeddings p_t from the CLIP text encoder and time embeddings t from a sinusoidal time encoder (Figure 1(a)). In parallel, the ControlNet branch receives the structural condition t0 and processes it through trainable copies of the SD encoder and middle blocks (Figure 1(b)). These control features are injected into the frozen decoder of the main diffusion stream via zero-convolution layers, enabling condition-guided and anatomically consistent reconstruction.

Built upon this architecture, BrainNormalizer is trained to reconstruct subject-specific pseudo-healthy MRIs from tumorous ones by imposing anatomical control guided by edge-based structural cues. In the first stage, the pretrained Stable Diffusion v1.5, originally trained on large-scale natural image datasets, is fine-tuned for domain adaptation to medical MRIs through inpainting-based reconstruction, as shown in Figure 2. Subsequently, a ControlNet is trained using Canny edge maps [46] as additional inputs while keeping the SD weights frozen, as illustrated in Figure 3. This process enhances edge-guided and anatomically faithful reconstruction, preserving subject-specific structural details. Finally, BrainNormalizer reconstructs a pseudo-healthy brain MRI from a tumorous input by leveraging a tricked prompt and a mirrored edge map, which jointly guide the model toward anatomically consistent, pseudo-healthy MRI reconstruction.

3.2 Stable Diffusion Fine-tuning

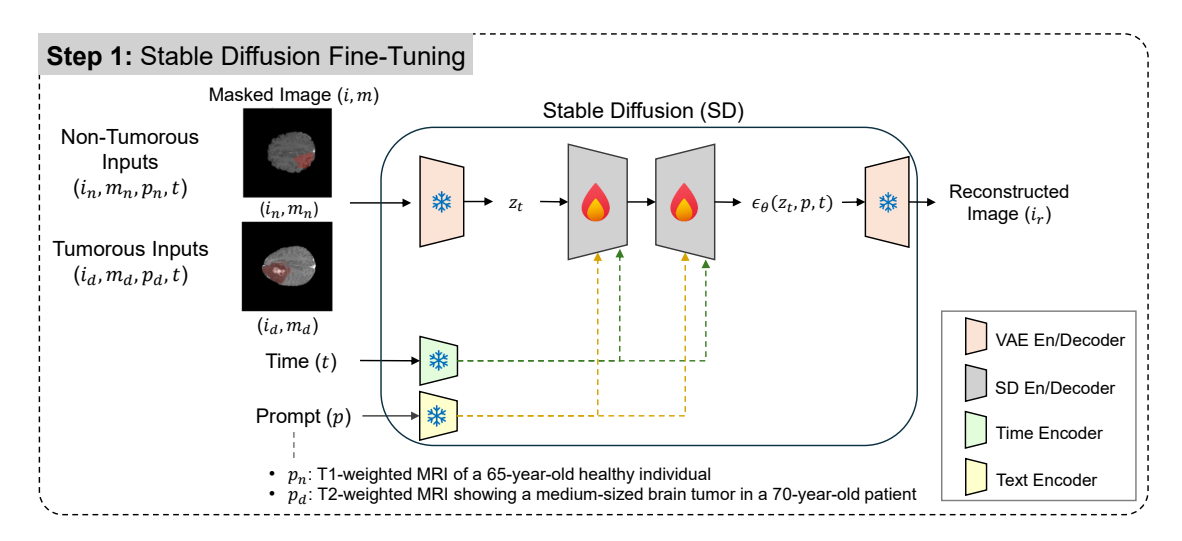


Figure 2: Step 1: Fine-tuning Stable Diffusion (SD). Both non-tumorous and tumorous MRI slices are provided as input pairs (i, m, p, t), consisting of a 2D image slice, binary mask, text prompt, and diffusion timestep. For non-tumorous inputs, a mask from a tumor slice with the same slice index is reused to maintain spatial consistency and robustness. The masked image is encoded into a latent representation z_t through the variational autoencoder (VAE) encoder, while the text prompt and timestep are embedded via the CLIP text encoder and time encoder, respectively. These embeddings are injected into the U-Net denoising network $\epsilon_{\theta}(z_t, p, t)$ within the SD framework, which predicts and removes noise to reconstruct the full image through the VAE decoder. **Abbreviations:** VAE, Variational Autoencoder; SD, Stable Diffusion.

As illustrated in Figure 2, the first stage of BrainNormalizer fine-tunes the pretrained SD to adapt it to the medical MRI domain through inpainting-based reconstruction. The SD backbone introduced in Section 3.1 is used here with its VAE, denoising U-Net, and cross-attention conditioning modules. During this stage, we freeze the pretrained VAE, CLIP text encoder, and noise scheduler, and fine-tune only the U-Net parameters to learn domain-specific MRI priors.

Both non-tumorous and tumorous cases are provided as independent input pairs (i, m, p, t), where i denotes the input 2D MRI slice, m the binary mask defining the inpainting region, p the text prompt, and t the diffusion timestep. For non-tumorous cases, the inputs are represented as (i_n, m_n, p_n, t) , where i_n is a non-tumorous MRI slice, m_n is the corresponding mask, and p_n is a prompt describing a normal brain structure. For tumorous cases, the inputs are represented as (i_d, m_d, p_d, t) , where i_d is a tumorous MRI slice, m_d is a binary tumor mask, and p_d is a prompt describing the presence and size of the tumor. Each input is constructed to reflect its clinical context, ensuring that the model learns to reconstruct anatomically plausible structures consistent with the semantic and spatial cues provided.

The binary mask m specifies the region of the image to be inpainted. For tumorous cases, the mask was derived from the ground-truth binary tumor mask and dilated by five pixels to ensure full coverage of the tumor boundaries. For non-tumorous cases, since no tumor masks are available, a mask was randomly borrowed from a tumorous slice with the same slice index to maintain spatial consistency and enhance robustness to mask variations. The masked image is obtained by applying m to i. This serves as the model input, where the masked region indicates the area to be reconstructed while the unmasked regions provide anatomical context for inpainting. During training, the loss is computed only within the masked region, ensuring that updates are focused on reconstructing the missing content while preserving the surrounding context.

Table 1: Prompt templates used for non-tumorous MRI cases. Non-tumorous prompts describe normal brain anatomy without pathological findings

Non-tumorous prompt

- 1. {modality} of a {age_desc} healthy individual.
- 2. A {age_desc} healthy person undergoing {modality}.
- 3. {modality} image of a healthy brain (age: {age_desc}).

Table 2: Prompt templates used for tumorous MRI cases. Tumorous prompts describe the presence and size of a tumor.

Tumorous prompt

- 1. {modality} of a {age_desc} patient with a {size_desc} tumor.
- 2. A {age desc} patient's {modality} scan showing a {size desc} tumor.
- 3. {modality} image showing a {size_desc} brain tumor in a {age_desc} patient.

The text prompt p provides semantic conditioning for each case and was generated from fixed template sets corresponding to the non-tumorous and tumorous cases. For both cases, a prompt was randomly selected from three predefined templates to prevent overfitting to a single phrasing pattern and to improve robustness to prompt variation during training. For non-tumorous MRIs, prompts were drawn from the templates in Table 1, parameterized by imaging modality and subject age. These prompts describe normal brain anatomy without pathological findings, for example, "T1-weighted MRI of a 65-year-old healthy individual" or "A T2-weighted MRI image of a healthy brain (age: 50)". For tumorous MRIs, prompts were generated from the templates listed in Table 2, parameterized by imaging modality, subject age, and tumor size. Tumor size categories were determined from pixel counts: small (1,000–1,400), mild (\sim 1,700), medium (\sim 2,000), moderate (\sim 2,300), and large (\sim 3,000). The resulting prompts semantically encode both age and tumor characteristics, such as "T2-weighted MRI showing a medium-sized brain tumor in a 70-year-old patient". When age information was unavailable, the placeholder unknown age was used.

The diffusion timestep t represents the noise level in the forward diffusion process, determining the degree of corruption applied to the latent representation before denoising-based reconstruction.

As depicted in Figure 2, each masked input image is encoded into a latent representation z_0 using the pretrained VAE encoder. Gaussian noise $\epsilon \sim \mathcal{N}(0, I)$ is then added according to a randomly sampled timestep t, which produces a noisy latent z_t following the diffusion forward process:

$$z_t = \sqrt{\bar{\alpha}_t} z_0 + \sqrt{1 - \bar{\alpha}_t} \epsilon,$$

where $\bar{\alpha}_t$ denotes the cumulative product of noise schedule coefficients. The text prompt p is transformed into text embeddings via the pretrained CLIP text encoder, and the timestep t is encoded using sinusoidal positional encoding. Both embeddings are injected into the U-Net through cross-attention and residual connections to provide semantic and temporal conditioning. The U-Net then predicts the added noise term as $\epsilon_{\theta}(z_t, p, t)$ based on these encoded representations. The loss function of SD fine-tuning minimizes the discrepancy between the true noise ϵ and the predicted noise $\epsilon_{\theta}(z_t, p, t)$ only inside the masked region, formulated as:

$$\mathcal{L}_{SD} = \mathbb{E}_{z_t, \epsilon, t, m} \left[\| m \odot (\epsilon - \epsilon_{\theta}(z_t, p, t)) \|_2^2 \right],$$

where \odot represents element-wise multiplication that restricts the loss computation to the masked area. After denoising, the latent is decoded by the VAE to reconstruct the full MRI image, with the masked region restored and the surrounding anatomy preserved.

By inpainting-based fine-tuning, the model learns to reconstruct both non-tumorous and tumorous cases in accordance with their semantic and anatomical contexts, leveraging text conditioning and pretraining.

3.3 ControlNet Training

After SD is fine-tuned through inpainting to capture general anatomical priors, the ControlNet is subsequently trained to provide subject-level anatomical guidance using edge information extracted from the input MRIs.

As shown in Figure 3, the ControlNet inherits the U-Net parameters from the fine-tuned SD model as a trainable copy, allowing it to leverage previously learned anatomical representations while processing additional edge information. For each input pair, the corresponding edge map c is extracted from the MRI slice using the Canny edge detector [46]. Canny edge detector is used for edge extraction due to its robust noise suppression and accurate localization enabled by Gaussian filtering and non-maximum suppression [47]. Specifically, c_n and c_d represent the edge maps for non-tumorous and tumorous cases, respectively, paired with $(i_n m_n, p_n)$ and (i_d, m_d, p_d) . These edge maps serve as

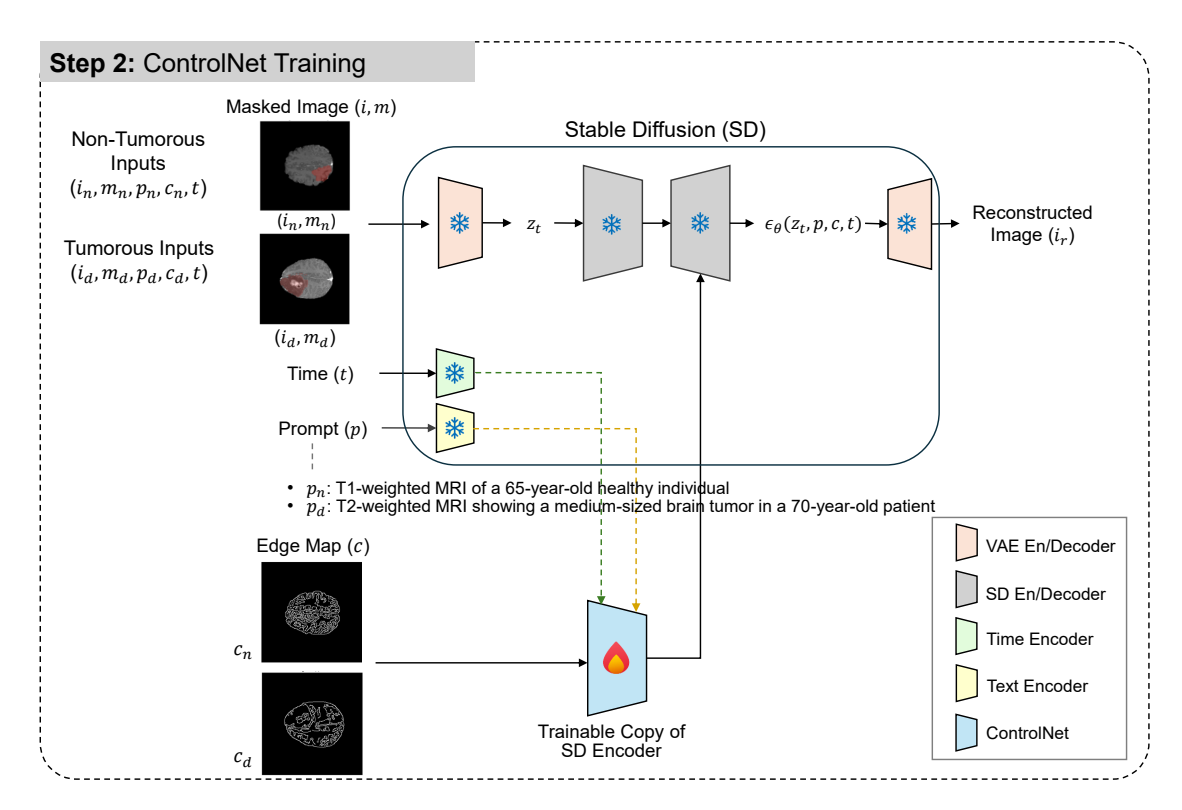


Figure 3: Step 2: ControlNet training for edge-guided anatomical reconstruction. ControlNet is built upon the fine-tuned SD model from Step 1. It receives the MRI slice, its binary mask, and the corresponding edge map c (either c_n or c_d). The ControlNet is initialized with the fine-tuned SD U-Net parameters, and their learned features are transmitted to the frozen SD decoder via zero-convolution layers (1 \times 1 convolutions initialized with zeros). **Abbreviations:** VAE, Variational Autoencoder; SD, Stable Diffusion.

additional conditioning inputs that capture fine anatomical boundaries relevant to each case. As illustrated in Figure 1, the ControlNet processes this edge-conditioned input to learn edge-guided structural features, which are then transmitted back to the frozen SD decoder through zero-convolution layers. The zero convolution layers are implemented as 1×1 convolutions with weights and biases initialized to zero, serving as controlled connections that gradually inject edge-aware features into the SD network. This design allows structural information to be seamlessly integrated into the generative process while preserving the anatomical priors obtained during SD fine-tuning.

The overall training objective of ControlNet follows the same denoising formulation as the SD fine-tuning stage, with the addition of the edge-conditioning term:

$$\mathcal{L}_{\text{ControlNet}} = \mathbb{E}_{z_t, \epsilon, t, c, m} \left[\| m \odot (\epsilon - \epsilon_{\theta}(z_t, p, t, c)) \|_2^2 \right],$$

where \odot represents element-wise multiplication restricting the loss computation to the masked area, and c represents the edge map. After denoising, the latent is decoded by the VAE decoder to reconstruct an anatomically coherent MRI image.

This objective allows the model to maintain the semantic consistency learned from SD while incorporating subject-specific structural cues provided by the edge map c, which enables anatomically faithful and structurally guided brain reconstruction.

3.4 Inference: Healthy Brain Generation

Pseudo-healthy brain generation is performed using the model trained through the two-stage process described in Section 3.2 and 3.3. As illustrated in Figure 4, we introduce a deliberate misalignment strategy between tumorous inputs and non-tumorous guidance to intentionally guide the model toward counterfactual healthy brain generation. For tumorous cases, the input configuration is deliberately adjusted to mislead the model's reconstruction objective: the model receives the tumorous slice i_d and its binary tumor mask m_d defining the inpainting region. The first component of the misaligned non-tumorous guidance provides a healthy-related prompt p_h selected from Table 1 for non-tumorous

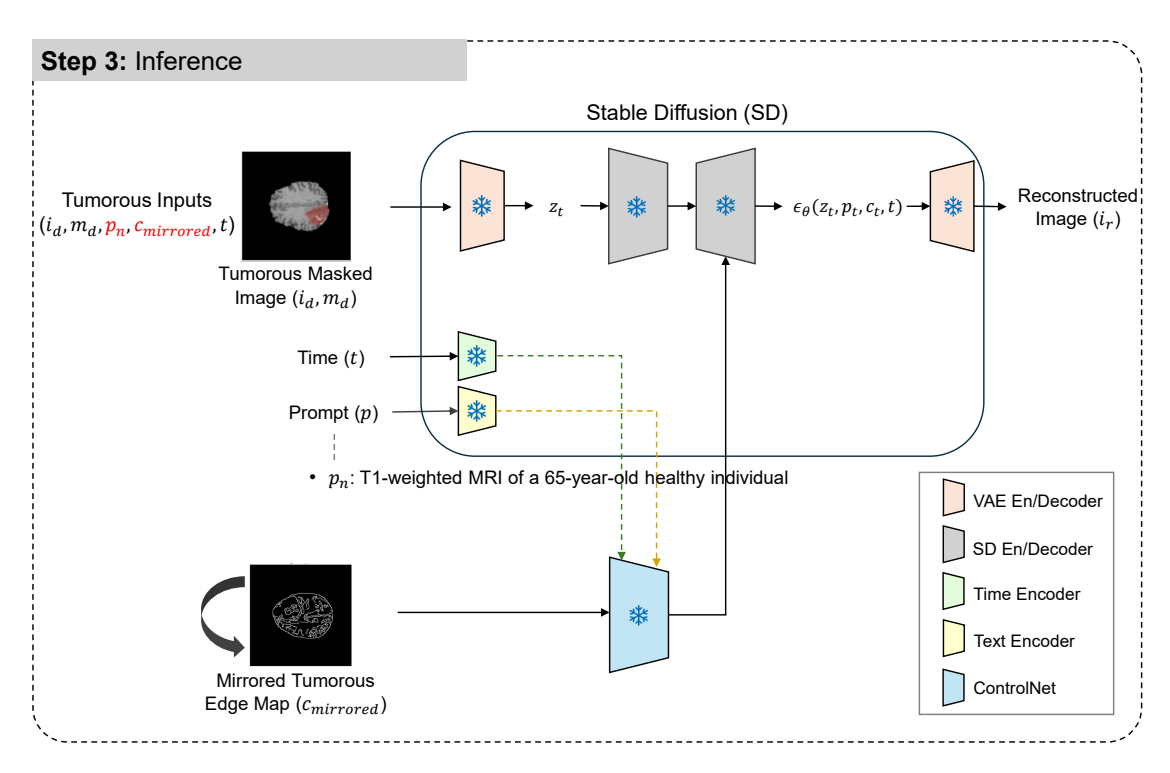


Figure 4: Step 3: Inference stage of BrainNormalizer. A deliberate misalignment strategy between tumorous inputs and non-tumorous guidance is applied to synthesize a pseudo-healthy brain. The model receives a tumorous slice i_d with its mask m_d , a non-tumorous prompt p_n , and a mirrored edge map $c_{\rm mirrored}$ to guide anatomically consistent reconstruction. **Abbreviations:** VAE, Variational Autoencoder; SD, Stable Diffusion.

inputs. This semantically guides the model to interpret the masked region as belonging to a non-tumorous brain. The second component relies on the general tendency for many major brain structures to show approximate contralateral symmetry, while recognizing that healthy brains are not perfectly symmetric and that tumors can introduce additional asymmetry [48]. A mirrored edge map $c_{\rm mirrored}$ is generated by mirroring the contralateral hemisphere, serving as a structural reference for the missing non-tumorous region. By incorporating this anatomical prior, the model aligns the reconstruction with the mirrored non-tumorous boundaries, producing anatomically plausible and spatially coherent replacements for tumorous regions.

4 Experiments

4.1 Dataset and Preprocessing

We used the BraTS2020 dataset, which contains multi-modal MRIs of brain tumor patients with MRI modalities: T1-weighted (T1), T2-weighted (T2), FLAIR, and T1-weighted with contrast enhancement (T1CE) and three tumor subregions (gadolinium-enhancing tumor, peritumoral edema, and necrotic and non-enhancing tumor core). In this study, only the T1CE modality was employed, which is a single-channel image providing the highest tumor-to-tissue contrast and the clearest delineation of enhancing tumor boundaries. This modality choice enables more reliable modeling of tumor-related structural patterns. All three tumor subregions were merged into a single "tumor" label to focus on the overall tumor extent rather than subregion-level differentiation. For each 3D volume, axial slices between indices 80 and 130 were extracted, covering the central brain region where tumors are typically observed. Images were clipped at the 99.5^{th} percentile of non-zero voxel intensities, zero-padded to a spatial size of 256×256 , and subsequently resized to 512×512 using nearest-neighbor interpolation to match the SD input resolution. To align with the model's expected three-channel input, each slice was channel-replicated. Image intensities were first normalized to the range [0,1] and subsequently rescaled to [-1,1], following the normalization procedure used in the original SD implementation.

Slices containing between 1,000 and 3,000 tumor pixels were categorized as tumorous, whereas slices with no tumor pixels were classified as non-tumorous. To prevent data leakage, the split was performed at the subject level, ensuring

that slices from the same subject were assigned exclusively to a single set. The dataset was divided into training and test sets with a 9:1 ratio, maintaining the ratio between non-tumorous and tumorous slices through stratified sampling. The training set comprised 330 subjects with 5,089 tumorous and 5,994 non-tumorous slices, resulting in a total of 11,083 slices. The test set included 35 subjects with 566 tumorous and 574 non-tumorous slices, for a total of 1,140 slices.

For edge extraction, we applied Canny edge detection after Gaussian smoothing with a kernel size of 5×5 and a standard deviation of $\sigma = 1.0$ to suppress high-frequency noise. The lower and upper thresholds for the Canny operator were set to 30 and 80, respectively.

4.2 Model Configuration and Training Hyperparameters

We adopted Stable Diffusion v1.5 (runwayml/stable-diffusion-v1-5) as the base architecture and initialized the model with publicly available pretrained weights. The model was fine-tuned in two sequential stages: (1) diffusion-based inpainting fine-tuning and (2) ControlNet fine-tuning with edge-guided structural conditioning.

For inpainting fine-tuning, we used a batch size of 8 with gradient accumulation over four steps, resulting in an effective batch size of 32. The model was trained for 30 epochs using the AdamW optimizer ($\beta_1 = 0.9$, $\beta_2 = 0.999$) with a weight decay of 0.01. The learning rate was set to 5×10^{-5} , decayed to zero following a cosine schedule without warm-up steps, and the gradient norm was clipped at 1.0 to ensure training stability. Text prompts were tokenized using the CLIP tokenizer, and each sequence was padded to the default maximum length of 77 tokens with [PAD] tokens. The gradient norm was clipped at 1.0 to maintain training stability.

For ControlNet fine-tuning, the same training configuration was adopted except for a higher learning rate of 5×10^{-4} and 500 warm-up steps to facilitate faster convergence. The model was trained for 20 epochs, reflecting the reduced number of trainable parameters compared to the inpainting stage. Except for the ControlNet branch and its zero-convolution layers, all other components (VAE, CLIP text encoder, and noise scheduler) remained frozen during training. This configuration allows the model to efficiently adapt to edge-guided structural conditioning while preserving the pretrained diffusion backbone.

4.3 Evaluation Protocol

Because paired non-tumorous ground truth is unavailable, pixel-level metrics are unsuitable for evaluating reconstruction quality. Minor pixel deviations caused by stochastic generation or noise do not necessarily indicate anatomical differences. Instead, we adopted perceptual and feature-level metrics that better capture realism and structural consistency.

To evaluate the effectiveness of each component, we compared three models: (1) a diffusion model based on DDIM sampling without inpainting or ControlNet conditioning proposed by Wolleb et al. [28], (2) a baseline diffusion model fine-tuned only with the first-stage inpainting objective, and (3) the proposed model with additional edge-guided ControlNet fine-tuning. This comparison enables an ablation-style assessment of the proposed edge-guided fine-tuning strategy.

To quantitatively evaluate model performance, we employed three complementary metrics that jointly assess image realism, structural integrity, and clinical plausibility.

Fréchet Inception Distance (FID). FID quantifies the distance between feature distributions of generated images and real non-tumorous images, computed in the feature space of a pretrained network:

$$FID = \|\mu_r - \mu_g\|_2^2 + Tr\left(\Sigma_r + \Sigma_g - 2(\Sigma_r \Sigma_g)^{1/2}\right),$$

where (μ_r, Σ_r) and (μ_g, Σ_g) denote the mean and covariance of features from real and generated images, respectively. Lower values indicate closer alignment to real-image distributions, reflecting higher perceptual realism and anatomical plausibility.

Structural Similarity Index (SSIM). SSIM measures local structural similarity between two images x and y in terms of luminance, contrast, and structure:

$$\mathrm{SSIM}(x,y) = \frac{(2\mu_x\mu_y + C_1)(2\sigma_{xy} + C_2)}{(\mu_x^2 + \mu_y^2 + C_1)(\sigma_x^2 + \sigma_y^2 + C_2)},$$

where μ_x , μ_y and σ_x^2 , σ_y^2 represent the local means and variances, and σ_{xy} the covariance between x and y. Given the absence of paired non-tumorous MRIs, SSIM was computed between the inpainted region and its contralateral non-tumorous region within each slice, serving as a proxy for evaluating structural symmetry preservation.

False Positive (FP) Detection Rate. A pretrained BraTS tumor segmentation model was used to evaluate clinical realism. The FP rate is defined as:

$$\text{FP Rate} = \frac{N_{\text{pred-tumor}}}{N_{\text{total}}},$$

where $N_{\text{pred-tumor}}$ denotes the number of generated non-tumorous slices predicted as containing tumors, and N_{total} the total number of generated slices. Lower FP rates indicate that the synthesized pseudo-healthy MRIs are less likely to be misclassified as tumorous, reflecting greater clinical plausibility.

4.4 Experiment Results

Table 3: Quantitative comparison of generative performance across different models. For each metric, lower FID and FP Segmentation values and higher SSIM indicate better performance.

Model	FID (↓)	SSIM (†)	FP Segmentation (↓)
Wolleb et al. [28]	43.1	0.37	15.7
SD Inpaint	32.5	0.68	10.4
BrainNormalizer (Proposed)	27.1	0.76	7.1

As shown in Table 3, the results demonstrate a clear performance improvement across models. Incorporating the tumorous mask for inpainting (SD Inpaint) substantially enhanced the realism and structural coherence of generated pseudo-healthy counterparts compared with the baseline diffusion model without inpainting or conditioning (Wolleb et al. [28]). Further fine-tuning with edge-guided ControlNet conditioning (BrainNormalizer) yielded additional gains, which confirms the benefit of structural guidance for more anatomically faithful reconstruction.

BrainNormalizer achieved the lowest FID of 27.1, indicating the closest alignment between the generated and real non-tumorous feature distributions. This substantial improvement reflects that structural conditioning not only enhances local anatomical realism but also aligns the overall feature statistics of the generated MRIs with those of authentic non-tumorous images. Compared with the baseline diffusion model (43.1) and SD Inpaint (32.5), this result demonstrates that mask-based inpainting and subsequent edge-guided fine-tuning together reduce distributional discrepancies, leading to more coherent and globally realistic reconstructions.

In terms of structural fidelity, BrainNormalizer achieved the highest SSIM of 0.76, showing a relative gain of 0.08 over SD Inpaint. This improvement suggests that the model produces smoother and more coherent structures with better boundary continuity. Because the SSIM was calculated between each reconstructed region and the contralateral non-tumorous half, this result highlights BrainNormalizer's strong ability to restore symmetric and anatomically consistent regions.

We further evaluated the clinical plausibility of the generated MRIs using a pretrained BraTS segmentation model as a downstream detector. BrainNormalizer achieved the lowest false positive (FP) detection rate of 7.1%, substantially lower than SD Inpaint (10.4%) and DDIM (15.7%). This low false positive rate indicates that BrainNormalizer successfully removed tumor-specific features while preserving non-tumorous tissue characteristics. In other words, our model produced realistic pseudo-healthy brain tissue that even fooled the specialized tumor detection model. This suggests that such clinically plausible counterfactuals could serve as reliable references for downstream clinical applications.

Figure 5 presents the reconstructed pseudo-healthy brain results for three representative subjects. BrainNormalizer demonstrated superior tumor-to-pseudo-healthy reconstruction while maintaining subject-specific anatomical geometry. The reconstruction results by Wolleb et al. [28] often left residual tumor signals and altered unrelated regions, indicating less targeted synthesis. In contrast, inpainting-based models such as SD-Inpaint and BrainNormalizer showed more localized changes concentrated within tumor areas, as evident in the difference maps. This suggests that inpainting helps preserve surrounding structural details. Although SD-Inpaint performs better than Wolleb et al. [28], it still exhibited incomplete tumor removal ((Figure 5(c))) and visible asymmetry in regions deformed by the tumor (Figure 5(a) and (b)). By incorporating edge-guided conditioning, BrainNormalizer achieved more symmetric and anatomically faithful reconstruction, as shown in Figure 5(a), and more complete tumor removal in Figure 5(c).

Both SD Inpaint and BrainNormalizer rely on inpainting-based reconstruction, which requires additional time and effort from clinicians to create binary tumor masks. To examine the impact of mask accuracy on reconstruction quality, we further performed pseudo-healthy brain reconstruction using expanded masks to simulate roughly annotated tumorous regions. Figure 6 compares the results of the two inpainting-based models, SD Inpaint and BrainNormalizer, under different mask settings. Across all three subjects, BrainNormalizer produced comparable pseudo-healthy reconstructions with both fine (default) and expanded masks, maintaining symmetry and effectively removing tumor regions. This

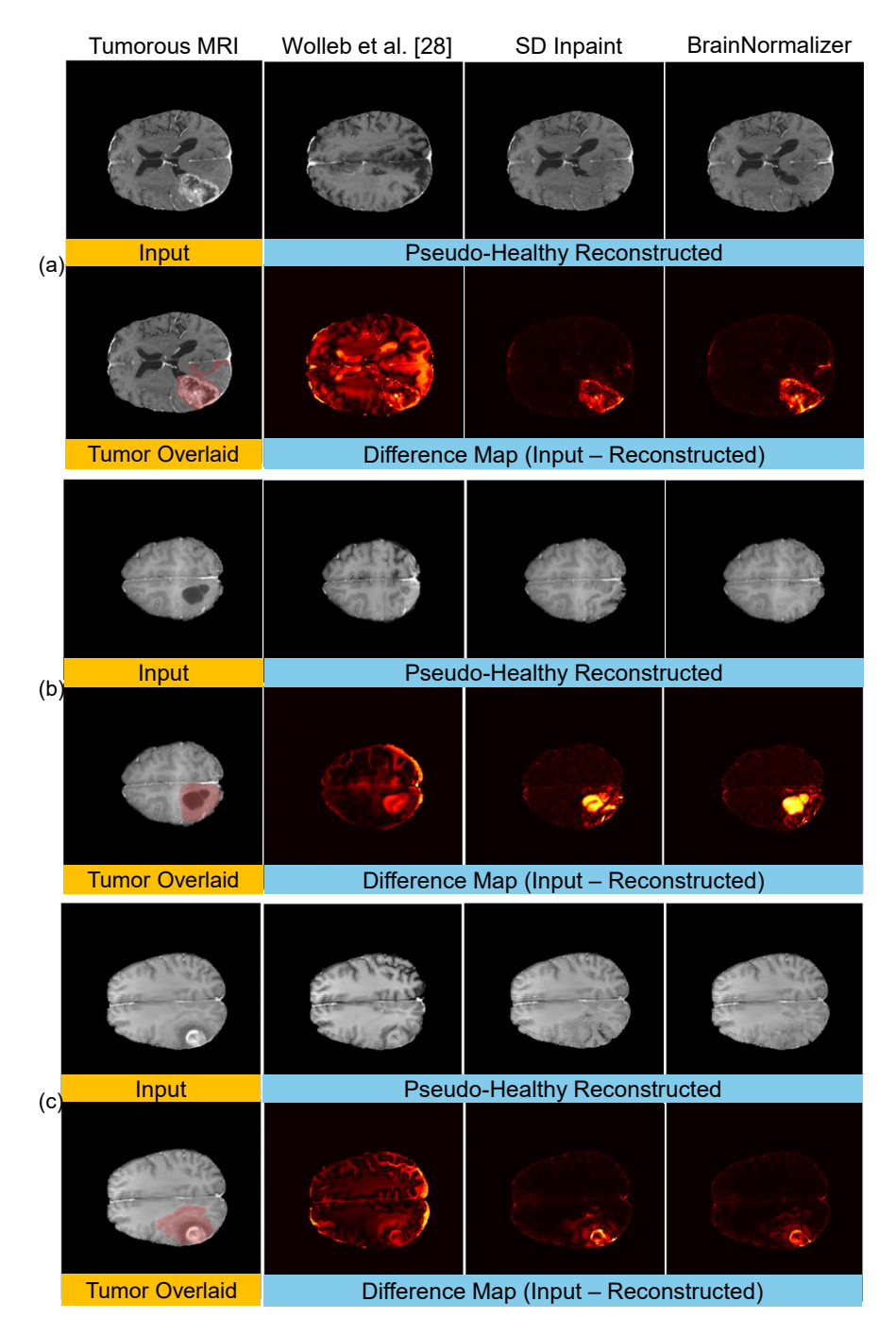


Figure 5: Visualization of pseudo-healthy brain reconstruction results for three representative subjects. Each pair of rows corresponds to the same subject: (a)–(c) show different cases. Columns show the tumorous MRI, reconstructed results by Wolleb et al. [28], SD Inpaint, and the proposed BrainNormalizer. The first row presents the input MRI and the corresponding pseudo-healthy reconstructed images, while the second row displays the tumor-overlaid input and the difference maps between the input and reconstructed images.

suggests robustness to mask imprecision. In contrast, SD Inpaint showed less precise tumor removal with expanded masks, occasionally leaving faint tumor remnants or introducing unnatural textures. This robustness suggests that BrainNormalizer could reduce the annotation burden for clinicians by tolerating less precise or coarsely defined masks.

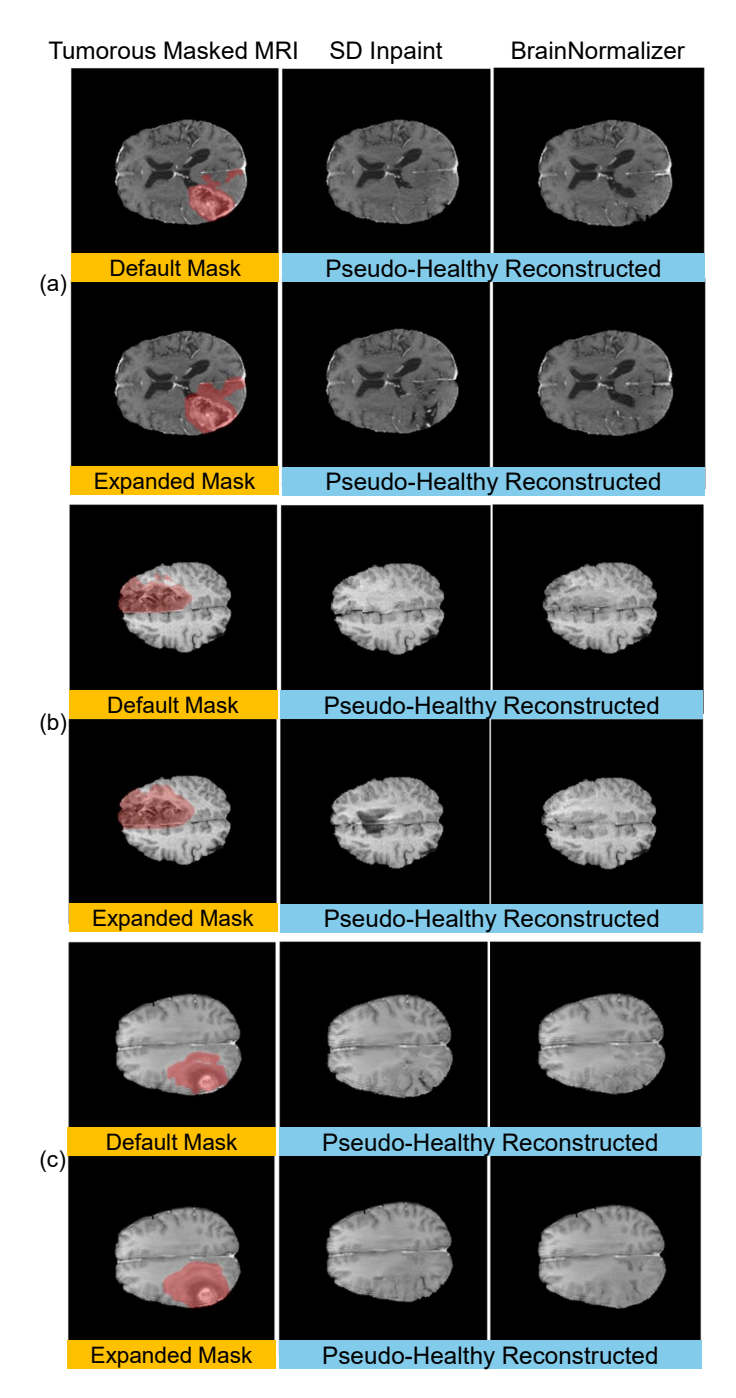


Figure 6: Visualization of mask-size robustness in pseudo-healthy brain reconstruction. Each pair of rows corresponds to the same subject MRI as in Figure 5, with (a), (b), and (c) showing three representative cases. The first row displays the ground-truth MRI overlaid with the default fine tumor mask and the corresponding pseudo-healthy results from each model. The second row shows results using an expanded mask that broadly covers the tumor region.

5 Conclusions

In this work, we presented BrainNormalizer, a diffusion-based framework that generates anatomically plausible pseudo-healthy brain MRIs from tumorous scans without requiring pairs of non-tumorous and tumorous data during training. Our work makes three key contributions. First, we introduce an anatomy-informed diffusion framework that incorporates structural guidance through edge-guided ControlNet conditioning, enabling subject-specific pseudo-

healthy brain reconstruction. Second, we propose a deliberate misalignment strategy that pairs tumorous inputs with non-tumorous prompts and mirrored contralateral edge maps during inference to generate anatomically plausible reconstructions. Third, from a clinical perspective, BrainNormalizer provides anatomically reliable reference images reflecting each subject's pseudo-healthy brain structure, facilitating accurate tumor delineation, preoperative planning, and longitudinal monitoring. By generating previously unavailable pairs of non-tumorous and tumorous MRI scans, our framework also enables new research in counterfactual modeling, tumor-induced deformation analysis, and personalized treatment planning. Quantitative evaluations on BraTS2020 demonstrate that BrainNormalizer outperforms existing methods in perceptual realism, structural fidelity, and clinical plausibility. Qualitative analyses confirm successful pseudo-healthy MRI generation while preserving subject-specific cortical geometry and ventricular morphology.

While demonstrating promising results, BrainNormalizer exhibits certain limitations. Reconstruction quality degrades when tumors occupy large central regions or affect both hemispheres simultaneously, as the contralateral hemisphere becomes less informative as a structural reference. Future work will explore several promising directions to address these challenges. First, integrating volumetric context through 3D diffusion backbones could leverage inter-slice consistency and improve reconstruction of large or contralateral tumors. Second, incorporating adaptive cross-hemisphere attention mechanisms may enable the model to better handle asymmetric tumor presentations. Third, extending the framework to multi-contrast MRI modalities (T1, T2, and FLAIR) could provide complementary anatomical information and enhance reconstruction robustness. Finally, clinical validation studies with radiologists and neurosurgeons would be essential to assess the practical utility of generated pseudo-healthy brain references in real-world treatment planning and surgical guidance workflows.

References

- [1] Lauren R Schaff and Ingo K Mellinghoff. Glioblastoma and other primary brain malignancies in adults: a review. *Jama*, 329(7):574–587, 2023.
- [2] Roger Stupp, Warren P Mason, Martin J Van Den Bent, Michael Weller, Barbara Fisher, Martin JB Taphoorn, Karl Belanger, Alba A Brandes, Christine Marosi, Ulrich Bogdahn, et al. Radiotherapy plus concomitant and adjuvant temozolomide for glioblastoma. *New England journal of medicine*, 352(10):987–996, 2005.
- [3] Quinn T Ostrom, Mackenzie Price, Corey Neff, Gino Cioffi, Kristin A Waite, Carol Kruchko, and Jill S Barnholtz-Sloan. Cbtrus statistical report: primary brain and other central nervous system tumors diagnosed in the united states in 2015–2019. *Neuro-oncology*, 24(Supplement_5):v1–v95, 2022.
- [4] Maurizio Cè, Giovanni Irmici, Chiara Foschini, Giulia Maria Danesini, Lydia Viviana Falsitta, Maria Lina Serio, Andrea Fontana, Carlo Martinenghi, Giancarlo Oliva, and Michaela Cellina. Artificial intelligence in brain tumor imaging: a step toward personalized medicine. *Current Oncology*, 30(3):2673–2701, 2023.
- [5] Joan Falcó-Roget, Alberto Cacciola, Fabio Sambataro, and Alessandro Crimi. Functional and structural reorganization in brain tumors: a machine learning approach using desynchronized functional oscillations. *Communications Biology*, 7(1):419, 2024.
- [6] Gagandeep Singh, Sunil Manjila, Nicole Sakla, Alan True, Amr H Wardeh, Niha Beig, Anatoliy Vaysberg, John Matthews, Prateek Prasanna, and Vadim Spektor. Radiomics and radiogenomics in gliomas: a contemporary update. *British journal of cancer*, 125(5):641–657, 2021.
- [7] Marc C Mabray, Ramon F Barajas Jr, and Soonmee Cha. Modern brain tumor imaging. *Brain tumor research and treatment*, 3(1):8, 2015.
- [8] James R Fink, Mark Muzi, Melinda Peck, and Kenneth A Krohn. Multimodality brain tumor imaging: Mr imaging, pet, and pet/mr imaging. *Journal of Nuclear Medicine*, 56(10):1554–1561, 2015.
- [9] Stefan Bauer, Roland Wiest, Lutz-P Nolte, and Mauricio Reyes. A survey of mri-based medical image analysis for brain tumor studies. *Physics in Medicine & Biology*, 58(13):R97, 2013.
- [10] Dhairya A Lakhani, David S Sabsevitz, Kaisorn L Chaichana, Alfredo Quiñones-Hinojosa, and Erik H Middle-brooks. Current state of functional mri in the presurgical planning of brain tumors. *Radiology: Imaging Cancer*, 5(6):e230078, 2023.
- [11] Mohamed L Seghier and Cathy J Price. Interpreting and utilising intersubject variability in brain function. *Trends in cognitive sciences*, 22(6):517–530, 2018.
- [12] Debadyuti Mukherkjee, Pritam Saha, Dmitry Kaplun, Aleksandr Sinitca, and Ram Sarkar. Brain tumor image generation using an aggregation of gan models with style transfer. *Scientific reports*, 12(1):9141, 2022.
- [13] Bhakti Baheti, Diana Waldmannstetter, Satrajit Chakrabarty, Mohammad Akbari, Michel Bilello, Benedikt Wiestler, Julian Schwarting, Evan Calabrese, Rudie Jeffrey, Syed Abidi, et al. The brain tumor sequence

- registration challenge: establishing correspondence between pre-operative and follow-up mri scans of diffuse glioma patients. *ArXiv. org*, (2112.06979), 2021.
- [14] Carsten Oliver Schmidt, Elizabeth Sierocinski, Sebastian-Edgar Baumeister, Katrin Hegenscheid, Henry Völzke, and Jean-François Chenot. Effects of whole-body mri on outpatient health service costs: a general-population prospective cohort study in mecklenburg-vorpommern, germany. *BMJ open*, 12(1):e056572, 2022.
- [15] Ian Goodfellow, Jean Pouget-Abadie, Mehdi Mirza, Bing Xu, David Warde-Farley, Sherjil Ozair, Aaron Courville, and Yoshua Bengio. Generative adversarial networks. *Communications of the ACM*, 63(11):139–144, 2020.
- [16] Zhiwen Liang, Mengjie Cheng, Jinhui Ma, Ying Hu, Song Li, and Xin Tian. Multimodal medical image-to-image translation via variational autoencoder latent space mapping. *Medical Physics*, 2025.
- [17] Jiayu Wang, Wengang Zhou, Jinhui Tang, Zhongqian Fu, Qi Tian, and Houqiang Li. Unregularized auto-encoder with generative adversarial networks for image generation. In *Proceedings of the 26th ACM international conference on Multimedia*, pages 709–717, 2018.
- [18] Matthew Cobbinah, Henry Nunoo-Mensah, Prince Ebenezer Adjei, Francisca Adoma Acheampong, Isaac Acquah, Eric Tutu Tchao, Andrew Selasi Agbemenu, Jerry John Kponyo, and Emmanuel Abaidoo. Diversity in stable gans: A systematic review of mode collapse mitigation strategies. *Engineering Reports*, 7(6):e70209, 2025.
- [19] Wenju Xu, Shawn Keshmiri, and Guanghui Wang. Adversarially approximated autoencoder for image generation and manipulation. *IEEE Transactions on Multimedia*, 21(9):2387–2396, 2019.
- [20] Biting Yu, Yan Wang, Lei Wang, Dinggang Shen, and Luping Zhou. Medical image synthesis via deep learning. Deep Learning in Medical Image Analysis: Challenges and Applications, pages 23–44, 2020.
- [21] Jonathan Ho, Ajay Jain, and Pieter Abbeel. Denoising diffusion probabilistic models. *Advances in neural information processing systems*, 33:6840–6851, 2020.
- [22] Jiaming Song, Chenlin Meng, and Stefano Ermon. Denoising diffusion implicit models. *arXiv preprint* arXiv:2010.02502, 2020.
- [23] Robin Rombach, Andreas Blattmann, Dominik Lorenz, Patrick Esser, and Björn Ommer. High-resolution image synthesis with latent diffusion models. In *Proceedings of the IEEE/CVF conference on computer vision and pattern recognition*, pages 10684–10695, 2022.
- [24] Amirhossein Kazerouni, Ehsan Khodapanah Aghdam, Moein Heidari, Reza Azad, Mohsen Fayyaz, Ilker Hacihaliloglu, and Dorit Merhof. Diffusion models in medical imaging: A comprehensive survey. *Medical image analysis*, 88:102846, 2023.
- [25] Firas Khader, Gustav Müller-Franzes, Soroosh Tayebi Arasteh, Tianyu Han, Christoph Haarburger, Maximilian Schulze-Hagen, Philipp Schad, Sandy Engelhardt, Bettina Baeßler, Sebastian Foersch, et al. Denoising diffusion probabilistic models for 3d medical image generation. *Scientific Reports*, 13(1):7303, 2023.
- [26] Aimon Rahman, Jeya Maria Jose Valanarasu, Ilker Hacihaliloglu, and Vishal M Patel. Ambiguous medical image segmentation using diffusion models. In *Proceedings of the IEEE/CVF conference on computer vision and pattern recognition*, pages 11536–11546, 2023.
- [27] Yijun Yang, Huazhu Fu, Angelica I Aviles-Rivero, Carola-Bibiane Schönlieb, and Lei Zhu. Diffmic: Dual-guidance diffusion network for medical image classification. In *International conference on medical image computing and computer-assisted intervention*, pages 95–105. Springer, 2023.
- [28] Julia Wolleb, Florentin Bieder, Robin Sandkühler, and Philippe C Cattin. Diffusion models for medical anomaly detection. In *International Conference on Medical image computing and computer-assisted intervention*, pages 35–45. Springer, 2022.
- [29] Nicholas Konz, Yuwen Chen, Haoyu Dong, and Maciej A Mazurowski. Anatomically-controllable medical image generation with segmentation-guided diffusion models. In *International Conference on Medical Image Computing and Computer-Assisted Intervention*, pages 88–98. Springer, 2024.
- [30] Jianhao Xie, Ziang Zhang, Zhenyu Weng, Yuesheng Zhu, and Guibo Luo. Meddiff-ft: Data-efficient diffusion model fine-tuning with structural guidance for controllable medical image synthesis. In *International Conference on Medical Image Computing and Computer-Assisted Intervention*, pages 306–316. Springer, 2025.
- [31] Gayatri Deshmukh, Onkar Kishor Susladkar, Debesh Jha, Elif Keles, Halil Ertugrul Aktas, Daniela P Ladner, Amir A Borhani, Gorkem Durak, Ulas Bagci, et al. Meddelinea: Scalable and efficient medical image segmentation via controllable diffusion transformers. In *Medical Imaging with Deep Learning*, 2025.
- [32] Alex Ling Yu Hung, Kai Zhao, Haoxin Zheng, Ran Yan, Steven S Raman, Demetri Terzopoulos, and Kyunghyun Sung. Med-cdiff: Conditional medical image generation with diffusion models. *Bioengineering*, 10(11):1258, 2023.

- [33] Hongxu Jiang, Muhammad Imran, Teng Zhang, Yuyin Zhou, Muxuan Liang, Kuang Gong, and Wei Shao. Fast-ddpm: Fast denoising diffusion probabilistic models for medical image-to-image generation. IEEE Journal of Biomedical and Health Informatics, 2025.
- [34] Le Zhang, Fuping Wu, Kevin Bronik, and Bartlomiej W Papiez. Diffuseg: domain-driven diffusion for medical image segmentation. *IEEE Journal of Biomedical and Health Informatics*, 2025.
- [35] Lvmin Zhang, Anyi Rao, and Maneesh Agrawala. Adding conditional control to text-to-image diffusion models. In *Proceedings of the IEEE/CVF international conference on computer vision*, pages 3836–3847, 2023.
- [36] Junde Wu, Rao Fu, Huihui Fang, Yu Zhang, Yehui Yang, Haoyi Xiong, Huiying Liu, and Yanwu Xu. Medsegdiff: Medical image segmentation with diffusion probabilistic model. In *Medical Imaging with Deep Learning*, pages 1623–1639. PMLR, 2024.
- [37] Zheyuan Zhang, Lanhong Yao, Bin Wang, Debesh Jha, Gorkem Durak, Elif Keles, Alpay Medetalibeyoglu, and Ulas Bagci. Diffboost: Enhancing medical image segmentation via text-guided diffusion model. *IEEE Transactions on Medical Imaging*, 2024.
- [38] Bram De Wilde, Anindo Saha, Maarten de Rooij, Henkjan Huisman, and Geert Litjens. Medical diffusion on a budget: textual inversion for medical image generation. *arXiv preprint arXiv:2303.13430*, 2023.
- [39] Yibo Zhao, Liang Peng, Yang Yang, Zekai Luo, Hengjia Li, Yao Chen, Zheng Yang, Xiaofei He, Wei Zhao, Qinglin Lu, et al. Local conditional controlling for text-to-image diffusion models. In *Proceedings of the AAAI Conference on Artificial Intelligence*, volume 39, pages 10492–10500, 2025.
- [40] Nejung Rue, Inye Na, Ho Yun Lee, and Hyunjin Park. Misalignment-aware mri-to-ct synthesis for lung segmentation on mri. In 2025 IEEE 22nd International Symposium on Biomedical Imaging (ISBI), pages 1–5. IEEE, 2025.
- [41] Kunpeng Qiu, Zhiqiang Gao, Zhiying Zhou, Mingjie Sun, and Yongxin Guo. Noise-consistent siamese-diffusion for medical image synthesis and segmentation. In *Proceedings of the Computer Vision and Pattern Recognition Conference*, pages 15672–15681, 2025.
- [42] Xiaojuan Liu, Cong Xiang, Libin Lan, Chuan Li, Hanguang Xiao, and Zhi Liu. Lesion region inpainting: an approach for pseudo-healthy image synthesis in intracranial infection imaging. *Frontiers in Microbiology*, 15:1453870, 2024.
- [43] Alicia Durrer, Philippe C Cattin, and Julia Wolleb. Denoising diffusion models for inpainting of healthy brain tissue. In *International Challenge on Cross-Modality Domain Adaptation for Medical Image Segmentation*, pages 35–45. Springer, 2023.
- [44] Dou Hoon Kwark, Shirui Luo, Xiyue Zhu, Yudu Li, Zhi-Pei Liang, and Volodymyr Kindratenko. Hierarchical diffusion framework for pseudo-healthy brain mri inpainting with enhanced 3d consistency. In MICCAI Workshop on Deep Generative Models, pages 78–88. Springer, 2025.
- [45] André Ferreira, Gijs Luijten, Behrus Puladi, Jens Kleesiek, Victor Alves, and Jan Egger. Brain tumour removing and missing modality generation using 3d wdm. *arXiv preprint arXiv:2411.04630*, 2024.
- [46] John Canny. A computational approach to edge detection. *IEEE Transactions on pattern analysis and machine intelligence*, (6):679–698, 2009.
- [47] Rui Sun, Tao Lei, Qi Chen, Zexuan Wang, Xiaogang Du, Weiqiang Zhao, and Asoke K Nandi. Survey of image edge detection. *Frontiers in Signal Processing*, 2:826967, 2022.
- [48] Xiang-Zhen Kong, Samuel R Mathias, Tulio Guadalupe, ENIGMA Laterality Working Group, David C Glahn, Barbara Franke, Fabrice Crivello, Nathalie Tzourio-Mazoyer, Simon E Fisher, Paul M Thompson, et al. Mapping cortical brain asymmetry in 17,141 healthy individuals worldwide via the enigma consortium. *Proceedings of the National Academy of Sciences*, 115(22):E5154–E5163, 2018.